Green Synthesis of New Heterocyclic Surfactant Compounds by Multicomponent Reactions and Their Antibacterial and Corrosion Inhibitor Study on Carbon Steel Alloy in Acid Media 2 M HCl

Raneen Salim Al-Hilfi[1], Najlaa Zaki Al-Ameri[2*], and Mouhanad Jwad Al-Asadi[1]

[1]*Department of Chemistry, College of Pure Science Education, University of Basrah, Basra 00964, Iraq*

[2]*Department of Second Party, Basra Oil Company (BOC) Iraqi Oil Ministry, Basra 00964, Iraq*

* ***Corresponding author:***

email: najlaa078@yahoo.com

Received: December 18, 2022
Accepted: February 19, 2023

DOI: 10.22146/ijc.80347

Abstract: *Heterocyclic 1,4-di(1,3,5-dithiazinan-5-yl)benzene (D) and two heterocyclic-cationic Gemini surfactant 5,5′-(1,4-phenylene)bis(5-decyl-1,3,5-dithiazinan-5-ium)bromide (E) and 5,5′-(1,4-phenylene)bis(5-tetradecyl-1,3,5-dithiazinan-5-ium)bromide (F) were prepared and identified by FTIR, ^{1}H-NMR spectroscopies, and GC–MS. Then, they were tested as corrosion inhibitors against carbon steel corrosion in 2.0 M aggressive HCl medium at 25 and 50 °C. They have different carbon chain tails, i.e., E (10 carbons), and F (14 carbons). These new heterocyclic and surfactant categories as corrosion inhibitors. The corrosion process has been studied electrochemically (Tafel Plot). The inhibition efficiency clarified that the decrease in IE(%) is in the order of F > E > D. The biological activity of compounds D and F was investigated using the aforementioned drilling procedure with a cork drill. At a dosage of 3000 mcg/mL, the biological action of compound D demonstrated effective resistance against the two types of negative bacteria. The cation has a diameter of 20 mm against* E. coli *and 19 mm against* S. epidermis *bacteria. At the same concentration, the chemical F is solely effective against* E. coli *with an inhibition diameter of 14 mm.*

Keywords: *antibacterial; carbon steel alloy; cationic Gemini; cyclothiomethylation; Tafel plot*

■ INTRODUCTION

The "green synthesis" approach of useful chemicals with minimal material, power, effort, and time costs has attracted much attention in recent years. One of these techniques is multicomponent reactions (MCRs), which allow for one-pot multistep synthesis without the requirement for intermediate separation and purification, hence decreasing chemical waste. Thiomethylation (reagent atom efficiency of 100% by the C, N, and S atoms) is the most efficient reaction in a sequence of "green" MCRs, yielding water as the only side product in addition to the target products [1-2]. Because of their chemical composition, organic corrosion inhibitors performed particularly well against steel corrosion. Some functional groups, such as oxygen, nitrogen, sulfur, phosphorous, and double bonds, may act as electronic-rich active sites for adsorption on the surface of corroded materials, thereby increasing steel protection [3-4].

The electronic-rich group can interact with the vacant *d*-orbital to form a protective layer, shielding the surface from the aggressive medium [5]. Surfactants have been shown to be promising corrosion inhibitors due to their unusual structure, which includes two opposing polarities: hydrophobic and hydrophilic portions at the same time. The hydrophilic heads, in particular, are electrically rich groups with a strong attraction to steel surfaces, whereas the hydrophobic surfactant tail acts as a protective coating [6-7]. Surfactants are used in various applications, including corrosion inhibitors, emulsifiers, drug technology, pharmaceutical formulation, nanotechnology, wetting agents, detergents, and catalyst technologies [8].

Gemini surfactants are identified by two identical parts separated by a spacer, each with the hydrophilic and lipophilic moieties. Compared to standard monomeric surfactants, this unusual structure governs their surface performance in solution. Gemini is a more effective surfactant with a lower critical micelle concentration (CMC) [4,7,9]. As a result, there has been a greater emphasis on developing innovative Gemini surfactants. Some of the novel Gemini surfactants have been created including heterocyclic cationic Gemini surfactants [4,9]. Because the former Gemini species has two hydrophilic heads with various charges, it can be classified as cationic-nonionic, anionic-nonionic, or anionic-cationic depending on its hydrophilic charges. Because of the changed charged ionic moiety, which lessens the repulsive force and allows for a closer distance, these unique categories result in a stronger adsorption tendency and a different aggregation structure than classic Gemini ones [10-11].

In this study, we prepared three inhibitors, named heterocyclic compounds and cationic heterocyclic Gemini surfactants with various carbon tails (D, E, and F). Electrochemical investigations were used to evaluate their corrosion resistance to steel corrosion. To our knowledge, these new heterocyclics and cationic heterocyclic Gemini surfactants were examined as corrosion inhibitors and antifungicidal agents for the first time. These new surfactants feature both positive and negative adsorption centers and several other electronic-rich function groups that may boost their adsorption capabilities. Electrochemical methods (Tafel plots) were used to study the steel surface, demonstrating the formation of a surfactant protective layer on the steel surface.

■ EXPERIMENTAL SECTION

Materials

All chemicals for the synthesis were commercially available with a purity of at least 97%: diaminobenzene ($C_6H_8N_2$, Sigma Aldrich), acetone ($(CH_3)_2CO$, Scharlau), 37% hydrochloric acid (HCl, B.D.H), 37% aqueous formaldehyde solution (CH_2O, Merck), 1-bromotetradecane ($C_{14}H_{29}Br$, Scharlau), 1-bromodecane ($C_{10}H_{21}Br$, Scharlau), ethanol (C_2H_5OH, B.D.H), sodium sulfide (Na_2S, Scharlau), dichloromethane (CH_2Cl_2, B.D.H), potassium hydroxide (KOH, B.D.H), and diethyl ether ($C_4H_{10}O$, Scharlau).

Instrumentation

The reaction products were identified using ^{1}H NMR spectra acquired on spectrometers (Bruker Avance 400 MHz), using internal standard TMS and DMSO-d_6 as the solvent. IR spectra were recorded on a Shimadzu, 84005 FTIR spectrometer, 400–4000 cm^{-1}, using KBr pellets. The melting point was determined by Thermo Scientific. GC-MS spectra were recorded on 5977 A MSD, Agilent 7890B GC device 70 eV, carrier gas helium, temperature program: rise from 40 to 300 °C at a rate of 10°/min. Individuality and purity of synthesized compounds were controlled using TLC on Silufol UV-254 plates; I_2 was used as a developer. Electrochemical measurements by Tafel polarization were carried out using Bank Elektronik-Intelligent Controls Type MLab 200.

Procedure

Steel composition and aggressive solution

The aggressive media was chosen to be 2 M HCl. It's made by diluting a concentrated HCl solution with doubly distilled water. The composition of the investigated steel specimen is shown in Table 1.

The examined steel was utilized in the electrochemical tests, with dimensions of 5 × 2 × 0.3 cm for length, width, and thickness, respectively. The SiC (grade 140, 320) was used to polish the carbon steel, which was then cleaned with distilled water, acetone, and completely dried in a desiccator [12].

Table 1. Components of the carbon steel alloy (C-95)

Element	Fe	C	Mn	P	S	Si	Cr	Ni	Cu	Mo	V
Percentage (%)	97.784	0.330	1.400	0.003	0.002	0.190	0.240	0.019	0.021	0.007	0.004

Potentiodynamic polarization experiments

This testing was performed using a three-electrode setup and an Auto lab. The polarization experiment was carried out by changing the inhibitor concentration (1×10^{-4}, 5×10^{-4}, 1×10^{-3}, 5×10^{-3}) at 25 and 50 °C.

Synthesis of 1,4-di(1,3,5-dithiazinan-5-yl)benzene (D)

The synthesis is carried out in two steps: First, formaldehyde (4.9 mL, 0.06 mol) and ethanol (50 mL) were added to a three-neck flask, followed by hydrogen sulfide (0.04 mol) bubbled with stirring for 30 min at room temperature [13-14]. The second step was dissolving diaminobenzene (1.08 g, 0.01 mol) in ethanol (50 mL) and dropwise addition to a water solution of formaldehyde (37%), saturating with H_2S with the diaminobenzene:H_2S:CH_2O ratio of 1:4:6. The mixture was refluxed for 48 h at 75 °C. The precipitate was then filtered and recrystallized with hot dichloromethane to get the target product D: Yield (70.0%) as a yellow crystal, m.p. (215–220 °C), as shown in Scheme 1 [13-16].

Synthesis of 5,5'-(1,4-phenylene)bis(5-decyl-1,3,5-dithiazinan-5-ium)bromide (E)

Compound D (1.6 g, 0.005 mol) was dissolved in the beaker with dichloromethane (20 mL), and then followed by the addition of 1-bromodecane (2.14 mL, 0.01 mol). For 24 h, the mixture was agitated on a magnetic stirrer at room temperature. The precipitate was then filtered, washed twice with diethyl ether, and air-dried to get the target product E: Yield (80.0%) as a yellow crystal, m.p. (200–205 °C), as shown in Scheme 1 [13,17].

Synthesis of 5,5'-(1,4-phenylene)bis(5-tetradecyl-1,3,5-dithiazinan-5-ium) bromide (F)

Compound D (1.6 g, 0.005 mol) was dissolved in the beaker with dichloromethane (20 mL), and 1-bromotetradecane (2.9 mL, 0.01 mol) was added to it. For 24 h, the mixture was stirred at room temperature. The precipitate was then filtered, washed twice with diethyl ether, and air-dried to get the target product E: Yield (87.5%) as a yellow crystal, m.p. (220–225 °C), as shown in Scheme 1 [13,17].

■ RESULTS AND DISCUSSION

Characterization of the Synthesized Compounds

Infrared spectrum of the compound D

We notice in Fig. S1 and Table 2 of the compound D the appearance of a band at 3051.39 cm^{-1} when it returns to the C–H vibration of the stretching of the aromatic bond of the benzene ring, and the appearance of two strong bands at 2970.38 and 2881.65 cm^{-1} and absorption bands with limits at 1419.16 and 1356.60 cm^{-1} due to shear vibration of the C–H aliphatic bond. The appearance of a weak bundle at 514.99 cm^{-1} to the C–S bond, a bundle at 1215.15 cm^{-1} return to the vibration of the stretching of the C–N wrist, and a bundle at 1660.71 cm^{-1} returns to stretching the C=C bond in the benzene ring.

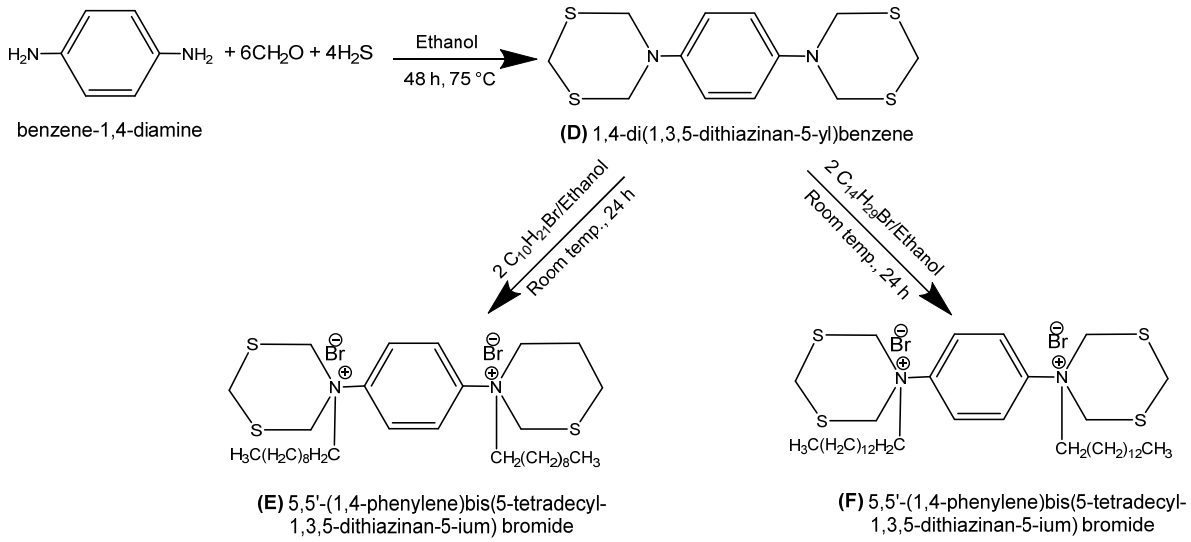

Scheme 1. Synthesis of heterocyclic and Gemini quaternary surfactants

Table 2. The most important bands in the infrared spectrum of the prepared compounds

Compd.	C–H Stretching aromatic (cm^{-1})	C–H Stretching aliphatic (cm^{-1})	C–H bending (cm^{-1})	C–S (cm^{-1})	C–N (cm^{-1})	C=C (cm^{-1})	N–H bending (cm^{-1})
D	3051.39	2970.38 & 2881.65	1419.16 & 1356.60	514.99 (w.b)	1215.15 (m)	1660.71 (m)	-
E	3039.81	2922.60 & 2850.79	1452.40 & 1363.67	551.64 (w.b)	1217.08 (m)	1656.85 (m)	-
F	3246.20	2922.16 & 2852.72	1452.40 & 1365.60	513.07 (w.b)	1215.15 (m)	1656.85 (m)	-

Infrared spectrum of the compound E

We observe in Fig. S3 and Table 2 of the compound E the appearance of a band at 3039.81 cm^{-1} for C–H vibration of the stretching of the aromatic bond of the benzene ring. The appearance of two strong bands at 2922.6 and 2850.79 cm^{-1} and absorption bands with limits at 1452.40 and 1363.67 cm^{-1} due to shear vibration of the aliphatic C–H bond. The appearance of a weak bundle at 551.64 cm^{-1} return to the C–S bond, a bundle at 1217.08 cm^{-1} for the vibration of the C–N stretching of the wrist, and a bundle at 1656.85 cm^{-1} for the stretching of C=C bond in the benzene ring.

Infrared spectrum of the compound F

We found in Fig. S5 and Table 2 of the compound F the appearance of a band at 3246.20 cm^{-1} for the C–H vibration of the stretching of the aromatic bond of the benzene ring. The appearance of two strong bands at 2922.16 and 2852.72 cm^{-1} and absorption bands at 1452.40 and 1356.60 cm^{-1} due to shear vibration of the aliphatic C–H bond. The appearance of a weak bundle at 513.07 cm^{-1} for the C–S bond, a bundle at 1215.15 cm^{-1} for the vibration of the C–N stretching of the wrist, and a signal at 1656.85 cm^{-1} returns to stretching the C=C bond in the benzene ring.

NMR spectrum of the compound D

The ^{1}H-NMR spectrum (Table 3 and Fig. S2) showed the appearance of a singlet signal at 3.55 ppm belonging to the protons of the carbon atom represented by the CH_2 group attached to two sulfur atoms and the number of 4 protons, and a single signal at 3.88 ppm represented by the CH_2 group attached to the sulfur and nitrogen atoms and the number of 8 protons, and a multiplet signal at 6.93–7.04 ppm refers to the protons of the aromatic ring and the number of 4 protons.

NMR spectrum of the compound E

The ^{1}H-NMR spectrum (Table 3 and Fig. S4) showed the appearance of a triplet signal at 0.83–0.86 ppm belonging to the protons of the carbon CH_3

Table 3. The most important signals appearing in the NMR spectrum of compounds D, E, and F

Signals	Chemical shift (ppm)	Chemical structures	Compound
(s, 4H, S-**CH_2**-S); (s, 8H, N-**CH_2**-S); (m, 4H, Ph-**H**)	3.55 3.88 6.93–7.04	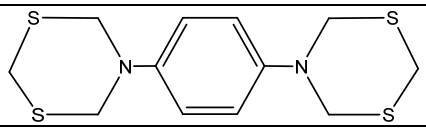	**D**
(t, 6H, $(CH_2)_8$**CH_3**); (m, 32H, **$(CH_2)_8$**CH_3); (t, 4H, N-**CH_2**); (s, 4H, S-**CH_2**-S); (s, 8H, N-**CH_2**-S); (m, 4H, Ph-**H**)	0.83–0.86 1.23–1.27 2.96–2.98 3.55 4.06 6.90–7.06	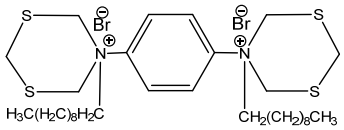 5,5'-(1,4-phenylene)bis(5-decyl-1,3,5-dithiazinan-5-ium) bromide	**E**
(t, 6H, $(CH_2)_{12}$**CH_3**); (m, 48H, **$(CH_2)_{12}$**CH_3); (t, 4H, N-**CH_2**); (s, 4H, S-**CH_2**-S); (s, 8H, N-**CH_2**-S); (m, 4H, Ph-**H**)	0.85–0.87 1.19–1.29 2.93–2.96 3.54 3.95 7.01–7.10	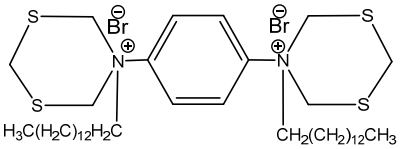 5,5'-(1,4-phenylene)bis(5-tetradecyl-1,3,5-dithiazinan-5-ium) bromide	**F**

represented by a group linked to the long chain $(CH_2)_8$ and the number of 6 protons. A multiplet signal at 1.23–1.27 ppm belonging to the protons of the carbon atom represented by the $(CH_2)_8$ group associated with the CH_3 group and the number of 32 protons. A triplet signal at 2.96–2.98 ppm referring to the protons of the carbon atom represented by the CH_2 group associated with the nitrogen atom and the number of 4 protons. A singlet signal at 3.55 ppm refers to the carbon atom represented by the CH_2 group attached to two sulfur atoms and the number of 4 protons and a singlet signal at 4.06 ppm represented by the CH_2 group attached to the sulfur and nitrogen atoms and the number of 8 protons. A multiplet signal at 6.90–7.06 ppm refers to the protons of the aromatic ring and the number of 4 protons.

NMR spectrum of the compound F

The ^{1}H-NMR spectrum (Table 3 and Fig. S6) was characterized by the appearance of a triplet signal at 0.85–0.87 ppm belonging to the protons of the CH_3 carbon represented by a group linked to the long chain $(CH_3)_{12}$ and the number of 6 protons, and a multiplet signal at 1.19–1.29 ppm belonging to the protons of the carbon atom represented by the $(CH_2)_{12}$ group associated with the CH_3 group and the number of 48 protons. A triplet signal at 2.93–2.96 ppm referring to the protons of the carbon atom represented by the CH_2 group associated with the nitrogen atom and the number of 4 protons. A singlet signal at 3.54 ppm refers to the carbon atom represented by the CH_2 group attached to two sulfur atoms and the number of 4 protons. A singlet signal at 3.95 ppm represented by the CH_2 group attached to the sulfur and nitrogen atoms and the number of 8 protons. A multiplet signal at 7.01–7.10 ppm refers to the protons of the aromatic ring and the number of 4 protons.

Mass spectrum of the prepared compounds

During our current study, the mass spectrum of the prepared compounds D, E, and F was recorded in order to prove their molecular formula (Tables 4–6 and Fig. 1–3) the aforementioned spectra showed a group of peaks of different molecular weights, with variation in their relative abundance as it gave a peak of fragmentation at m/z = 781.1, 758.6, and 316.1 with their relative abundance ranged (13.5, 9.32, and 2.26%) which is due to the parent molecular ion of the compounds D, E, and F, respectively.

Potentiodynamic Polarization Studies

Tables 7 and 8 illustrate the polarization of carbon steel alloy corrosion in the absence and presence of various dosages (1×10^{-4}, 5×10^{-4}, 1×10^{-3}, 5×10^{-3}) M of D, E, and F inhibitors at 25 and 50 °C. Fig. 4–8 illustrate the polarization curves. According to the data, the uninhibited sample had the maximum corrosion current density. However, when the inhibitor concentration rises, so does the corrosion current density, I_{corr} (μA cm^{-2}). Corrosion rate CR (mpy) values exhibit the same tendency as current density, with values decreasing as inhibitor concentration increases. The

Table 4. The important fragments and relative abundance of the compound D

Fragments	m/z	% Relative abundance
$[M]^+$	316.1	13.5
$[C_{11}H_{11}N_2S_3]^+$	267.2	2.7
$[C_{10}H_{12}N_2S_2]^+$	224.1	6.5
$[C_8H_4NS_2]^+$	178.1	3.5
$[C_8H_4NS]^+$	146.1	9.2
$[C_8H_8N_2]^+$	132.1	14.1
$[C_8H_8N]^+$	118.1	7.7

Table 5. The important fragments and relative abundance of the compound E

Fragments	m/z	% Relative abundance
$[M]^+$	758.6	9.3
$[C_{32}H_{58}N_2S_4Br]^+$	679.0	13.9
$[C_{11}H_{13}N_2S_4]^+$	301.2	1.3
$[C_{10}H_{17}N_2S_2]^+$	229.0	20.8
$[C_8H_3NS_2]^+$	177.1	13.9

Table 6. The important fragments and relative abundance of the compound F

Fragments	m/z	% Relative abundance
$[M]^+$	871.1	2.6
$[C_{40}H_{78}N_2S_4]^+$	711.1	5.3
$[C_{26}H_{67}N_2S_4]^+$	535.5	1.7
$[C_{22}H_{79}N_2S_4]^+$	341.2	8.9
$[C_{10}H_{23}N_2S_3]^+$	267.2	10.9
$[C_7H_{25}NS_2]^+$	137.1	14.3

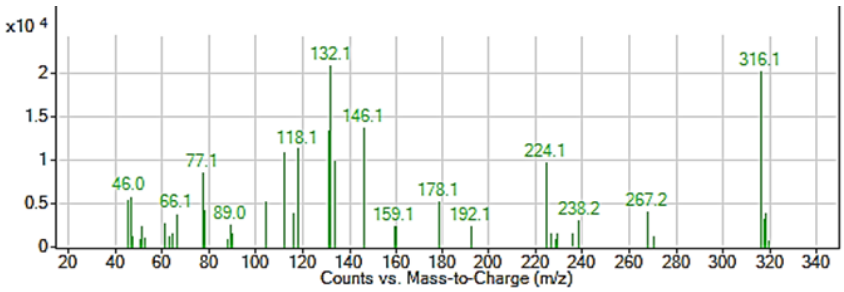

Fig 1. Mass spectrum of the synthesized heterocyclic compound D

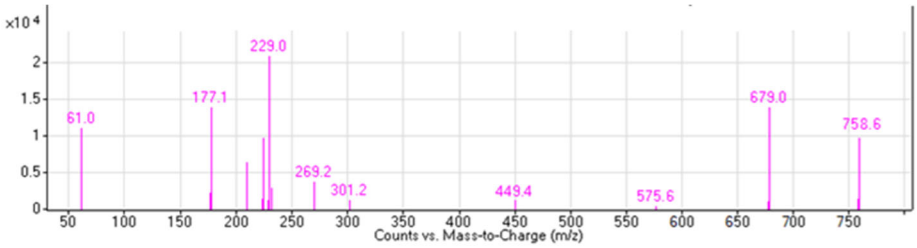

Fig 2. Mass spectrum of the synthesized heterocyclic - Gemini surfactant E

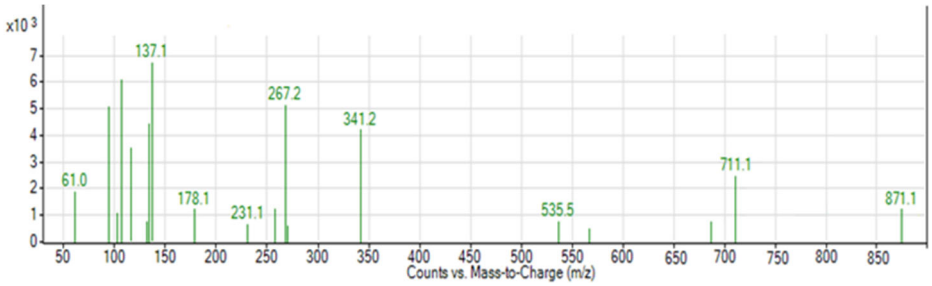

Fig 3. Mass spectrum of the synthesized heterocyclic-Gemini surfactant F

Table 7. Tafel polarization parameters in the absence and presence of various concentrations of inhibitors for carbon steel C95 in 2 M HCl at 298 K

Inhibitor	Conc. of inhibitor (M)	$-E_{corr}$ (mV)	CR (mpy)	I_{corr} ($\mu A\ cm^{-2}$)	β_c ($mV\ dec^{-1}$)	β_a ($mV\ dec^{-1}$)	IE%	Θ
D	0	462.80	14.81	32.56	−198.20	193.00	-	-
	1×10^{-4}	470.50	5.99	13.18	−223.60	197.20	59.50	0.59
	5×10^{-4}	415.40	4.51	9.90	−187.30	206.40	69.50	0.69
	1×10^{-3}	468.60	3.89	8.55	−196.60	150.20	73.70	0.73
	5×10^{-3}	377.50	1.42	3.13	−145.70	78.10	90.30	0.90
E	0	462.80	14.81	32.56	−198.20	193.00	-	-
	1×10^{-4}	446.10	5.99	13.17	−141.90	192.00	59.50	0.59
	5×10^{-4}	460.80	4.82	9.41	−222.10	158.20	71.20	0.71
	1×10^{-3}	375.30	2.97	6.53	−197.40	204.60	79.90	0.79
	5×10^{-3}	529.90	1.32	2.90	−203.90	293.10	91.00	0.91
F	0	462.80	14.81	32.56	−198.20	193.00	-	-
	1×10^{-4}	441.20	5.93	13.05	−208.60	163.20	59.90	0.59
	5×10^{-4}	390.30	2.93	6.45	−201.90	121.60	80.10	0.80
	1×10^{-3}	370.60	1.04	5.55	−142.40	68.60	83.00	0.83
	5×10^{-3}	433.70	1.03	2.28	−162.00	119.80	92.90	0.92

Table 8. Tafel polarization parameters in the absence and presence of various concentrations of inhibitors for carbon steel C95 in 2 M HCl at 323 K

Inhibitor	Conc. of inhibitor (M)	$-E_{corr}$ (mV)	CR (mpy)	I_{corr} (μA cm^{-2})	β_c (mV dec^{-1})	β_a (mV dec^{-1})	IE%	Θ
D	0	445.80	25.68	56.44	−171.70	148.30	-	-
	1×10^{-4}	519.20	14.56	32.00	−227.50	338.70	43.30	0.43
	5×10^{-4}	452.30	9.85	21.67	−200.50	163.50	61.60	0.61
	1×10^{-3}	468.50	8.24	18.12	−160.60	144.20	67.80	0.67
	5×10^{-3}	476.10	6.38	14.04	−288.20	240.80	75.10	0.75
E	0	445.80	25.68	56.44	−171.70	148.30	-	-
	1×10^{-4}	377.80	10.90	24.08	−210.30	250.90	57.30	0.57
	5×10^{-4}	501.40	9.41	20.70	−238.30	197.50	63.30	0.63
	1×10^{-3}	372.00	7.80	17.15	−251.80	195.80	69.60	0.69
	5×10^{-3}	354.40	2.04	9.49	−159.80	158.00	83.10	0.83
F	0	445.80	25.68	56.44	−171.70	148.30	-	-
	1×10^{-4}	373.80	10.72	23.58	−199.30	123.40	58.20	0.58
	5×10^{-4}	404.30	5.14	11.31	−225.00	137.10	79.90	0.79
	1×10^{-3}	376.30	2.68	9.91	−228.80	124.10	82.40	0.82
	5×10^{-3}	424.80	1.92	8.28	−177.60	114.80	84.30	0.84

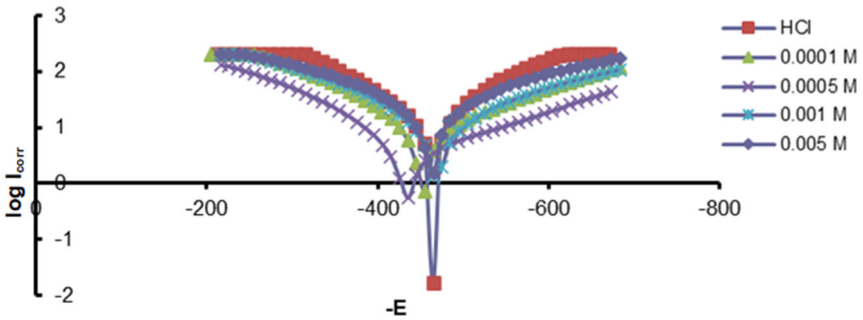

Fig 4. The potentiodynamic polarization curve for C95 alloy in (2 M HCl solution + various concentrations of compound D) at 298 K

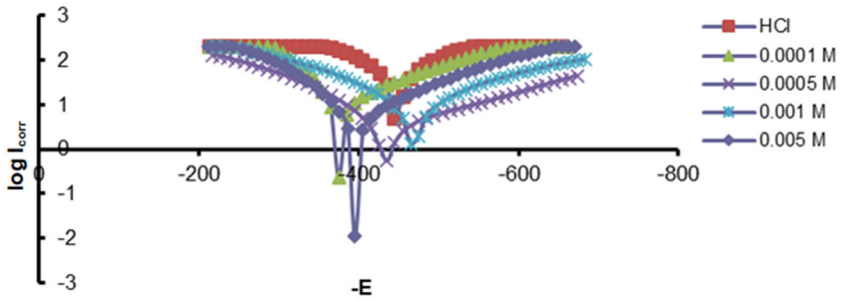

Fig 5. The potentiodynamic polarization curve for C95 alloy in (2 M HCl solution + various concentrations of compound D) at 323 K

obtained inhibitor efficiency followed a similar trend, as previously stated. All of this suggests that as the concentration of the inhibitor increases, so does its efficacy [17-23]. Adsorption of sulfur atoms in inhibitors (D, E, and F) on the steel surface, and surfactants that represent the CR, is referred to as dropping the CR (E and F). The adsorption process improves as the inhibitor concentrations rise [24].

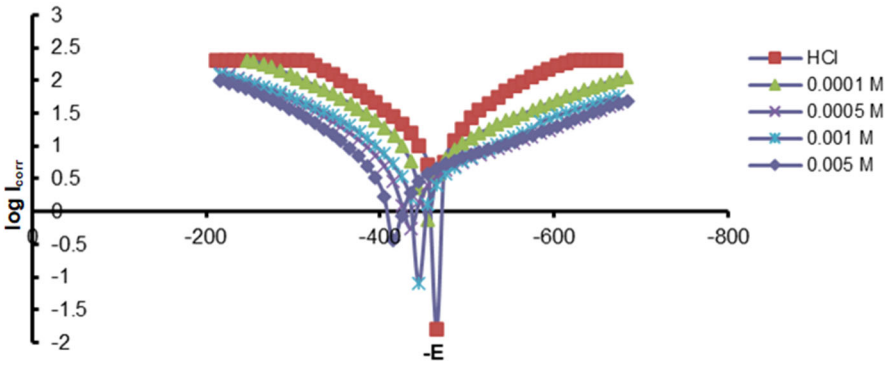

Fig 6. The potentiodynamic polarization curve for C95 alloy in (2 M HCl solution + various concentrations of compound E) at 298 K

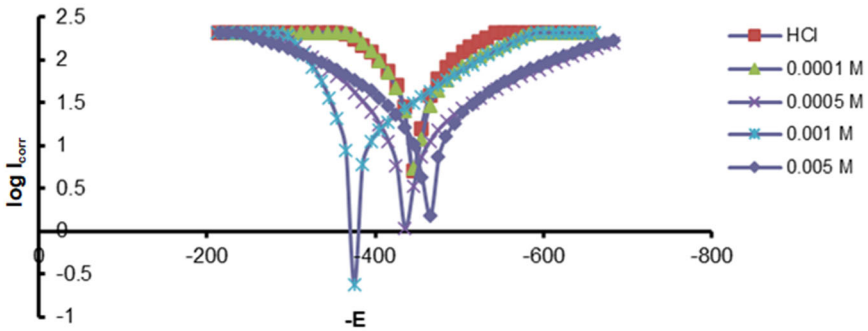

Fig 7. The potentiodynamic polarization curve for C 95 alloy in (2 M HCl solution + various concentrations of compound E) at 323 K

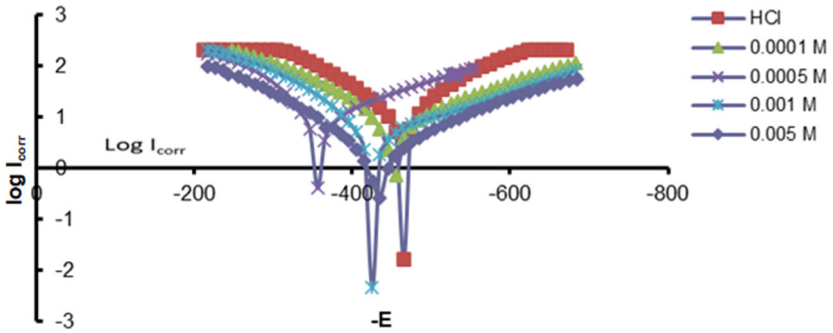

Fig 8. The potentiodynamic polarization curve for C 95 alloy in (2 M HCl solution + various concentrations of compound F) at 298 K

The adsorption of D, E, and F on the steel surface creates a protective barrier that keeps the steel surface from being corroded. Steel protection is improved by increasing the concentration of surfactant-inhibitors [17,24]. The findings also show that the inhibitory passivity gradually increased, caused by the inhibitor's passive film clinging to the electrode surface. Because there is variance in both cathodic (βc), and anodic (βa) responses when compared to blank, both cathodic and anodic reactions are inhibited with the administration of inhibitors [25-27]. When the displacement of corrosion potential (E_{corr}) from the corrosion potential of the blank exceeds 85 mV, the inhibitor is either cathodic or anodic. If the displacement in (E_{corr}) is less than 85 mV, the corrosion inhibitor is of the mixed type [28-29]. The displacements in (E_{corr}) in the current study are 85.3, 67.1, and 29.1 mV for D, E, and F, respectively, as calculated by Eq. (1).

$$\%IE = I^{\circ}_{corr} - I_{corr} I^{\circ}_{corr} \times 100 \quad (1)$$

where: I°_{corr} and I_{corr} is corrosion current density in the absence and presence of inhibitors, respectively. As a result, the inhibitors tested (E and F) are mixer kinds, with (D) being somewhat more cathodic or anodic as shown in Fig. 4–8 [23,27].

The following Eq. (2) and (3) [17,27,29] can be used to assess inhibitory efficiency.

$$\%IE = \left(\frac{I^{\circ}_{corr} - I_{corr}}{I_{corr}} \right) \quad (2)$$

$$\theta = \frac{I^{\circ}_{corr} - I_{corr}}{I_{corr}} \quad (3)$$

The corrosion rate (CR mpy) of a carbon steel alloy (C95) in an acidic solution in the absence and presence of varied concentrations of heterocyclic organic compounds as inhibitors and within the temperatures (298, 323 K) was estimated using the following Eq. (4) [17,27,29].

$$CR = K \times \frac{I_{corr}}{\rho} \times EW \quad (4)$$

The surfactant-inhibitor results (Tables 7 and 8, Fig. 6-9) show how inhibition effectiveness affects the hydrophobic structure. Increasing the hydrophobic nature of the surfactant tail elongation increases the steel inhibition efficacy. Surfactant F is more effective than surfactant E because it has a tail with 14 carbon atoms, whereas E has just a tail with 10 carbon atoms [30-31]. For example, at a concentration of 5×10^{-3} M, the IE% of inhibitors E and F at 25 °C is 66.6 and 68.1%, respectively (Table 7). As previously noted, increasing the carbon tail length increases surface adsorption affinity [31-32]. As a result, the surfactant tail modulates surfactant inhibitor adsorption on the surface, increasing surface coverage and inhibition effectiveness [33-35].

The temperature has a major impact on the performance of the inhibitors investigated. Temperature increases of the corrosive solution containing the synthesized D, E, and F inhibitors enhanced the steel's corresponding CR, as indicated in Tables 7 and 8. The findings demonstrate a constant increase in CR as the temperature of the solution rises, confirming the presence of the investigated D, E, and F inhibitors [32,35]. The growing CR with temperature trend reflects the affinity of the generated inhibitors for chemical adsorption on the steel surface. The chemical structure of the E and F Gemini surfactant-inhibitors changed as the solution temperature increased, resulting in larger electronic densities of the active centers and, as a result, higher adsorption on the corroded surface [36-37]. The negatively charged center of the inhibitors generated interacts electrostatically with the negatively charged center formed on the surface of steel after it has been dipped in a vigorous acidic solution [12,38].

Inhibition Mechanism

The adsorption of these compounds to the metal solution interface could explain why D, E, and F have an inhibitory effect on the corrosion of carbon steel in 2 M HCI solution. The nature of the metal, the chemical structure of the inhibitors, the inhibitor concentration, the inhibitor active sites, the electronic cloud, the composition of the electrolyte, and the temperature influence the amount of inhibitor adsorption [39]. Adsorption on the metal surface was proposed to occur via the active center present on inhibitor molecules and to be charge density dependent, as shown in Schemes 2–4 [4,40].

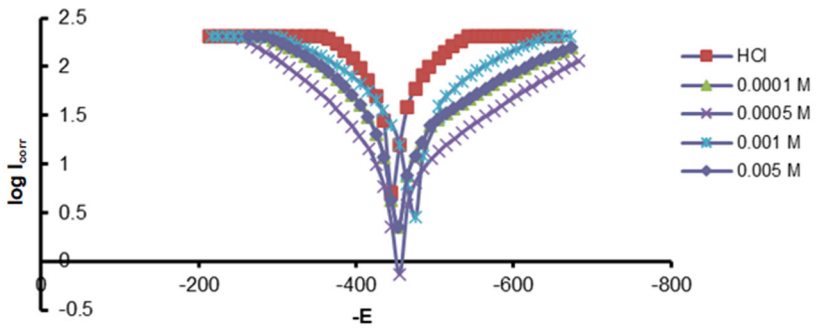

Fig 9. The potentiodynamic polarization curve for C 95 alloy in (2 M HCl solution + various concentrations of compound F) at 323 K

According to the inhibition efficiency, the decline in %IE occurs in the following order: F > E > D. Compound F (designed as 14-pH-14) has a stronger adsorption propensity on interfaces than the shorter chain surfactant E (designed as 10-pH-10) and thus has a slightly better inhibitory impact on corrosion than compound E [30,39]. The surfactant tail essentially increases adsorption at interfaces, promoting their activity as corrosion inhibitors. As a result, the surfactant tail increases the adsorption proclivity on the steel surface, delaying the attack of the corrosive solution. The positively charged quaternary ammonium nitrogen interacts electrostatically with the bridging negatively charged (Cl^-) ions on the positively charged metal surface to form a protective layer that isolates the surface from contact with an aggressive medium, thereby slowing steel corrosion, as shown in Schemes 2–4 [17,40].

Furthermore, our synthesized aromatic heterocyclic inhibitors had several electronic rich functional groups such as N, S, C–N, and C=C that might interact with the iron's unoccupied *d*-orbital and improve their adsorption effectiveness on the tested carbon steel [13,41]. In this scenario, the inhibitory effect is caused by the interaction of the π-electron and the existence of an electron donor for four sulfur atoms, which forms a connection with the metal atom's unoccupied *d*-orbital at the interface.

In general, two adsorption mechanisms on the metal surface in acid media are examined [13]. In the first model, neutral molecules may be adsorbed on the surface of carbon steel via the chemisorption mechanism, which involves the displacement of water molecules from the surface of carbon steel and the sharing of electrons between heteroatoms and iron [39,42]. Based on donor-acceptor interactions between their π-electrons and unoccupied *d*-orbitals of surface iron, inhibitor molecules may likewise be adsorbed on the carbon steel surface [13].

In the second model, it is well known that electrostatic repulsion makes it difficult for protonated molecules to approach the positively charged carbon steel surface. Because Cl^- has a lower degree of hydration, it may bring excess negative charges near the interface, allowing for more adsorption of positively charged inhibitor molecules. Protonated inhibitors adsorb via electrostatic interactions between positively charged molecules and the negatively charged metal surface. As a result, adsorbed Cl^- ions and protonated inhibitors work together [4,43].

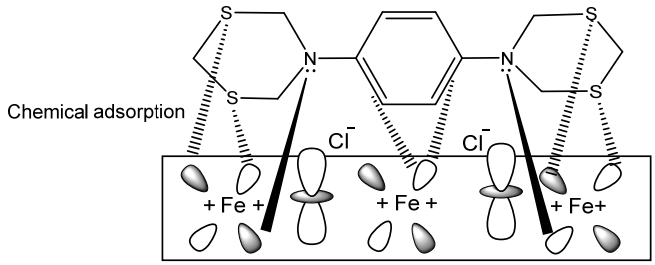

Scheme 2. Adsorption of the synthesized inhibitor D on the steel surface is predicted

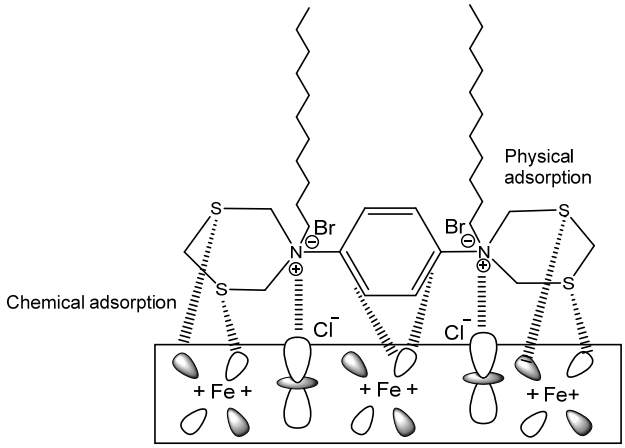

Scheme 3. Adsorption of the synthesized inhibitor E on the steel surface is predicted

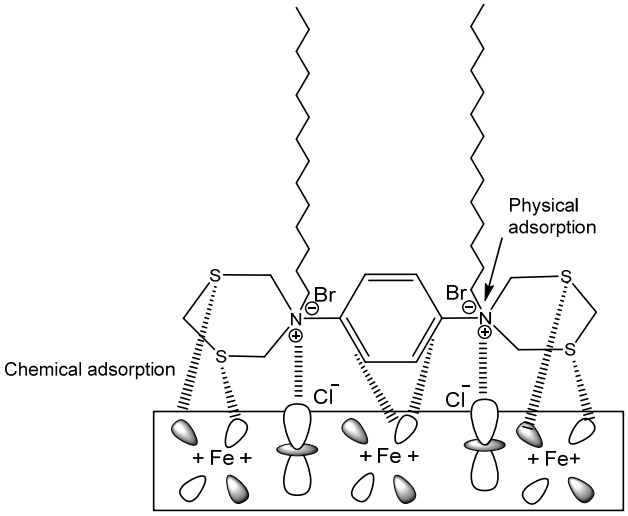

Scheme 4. Adsorption of the synthesized inhibitor F on the steel surface is predicted

Biological Assay

The tendency of their remedies to disintegrate the outer cell wall, resulting in the exudation of cell fluids and the death of pathogenic bacteria, makes heterocyclic compounds physiologically efficient in suppressing many different types of pathogenic bacteria [44]. The existence of unique active groups within the composition of cyclic compounds, such as groups C–S, C–N, and NH_2 may result in the formation of complexes with elements in the cell body, such as copper, iron, and divalent cobalt ions, which leads to cell death owing to their loss, these are the items [44].

Because of the existence of a form of corrosion induced by bacteria in the ground (in reservoir water and oil) that convert some sulfur-containing oil molecules to H_2S, SO_2, and SO_3, which degrades metals by converting them to sulfurous acid in the presence of water, which is one of the reasons. Because heterocyclic compounds include nitrogen and sulfur atoms that differentiate them for associating with various elements, much and ongoing research have been undertaken in the field of suppressing various forms of bacteria, i.e., negative for cream dye (*S. epidermis*) and positive for cream dye (*E. coli*) [44-45].

The aforementioned drilling procedure was used in conjunction with a cork drill, and the damping diameters were measured in millimeters using a ruler. The results demonstrated the biological action of solutions of various chemicals generated from it with the bacteria under research at a concentration of 1000 ppm. The compound D demonstrated effective resistance to both types of negative bacteria. At a concentration of 3000 mcg mL^{-1}, the cation has a diameter of 20 mm against *E. coli* bacteria and 19 mm against *S. epidermis* bacteria. At the same concentration, the compound F is solely effective against gram-negative bacteria (*E. coli*), with an inhibition diameter of 14 mm, as shown in Fig. 10 and 11 [46].

It was discovered that the complexes had a stronger inhibitory efficiency than the ligands based on the results provided in Table 9 arising from the action of the produced compounds against the specified species of bacteria. The effects of metal on normal biological processes [46].

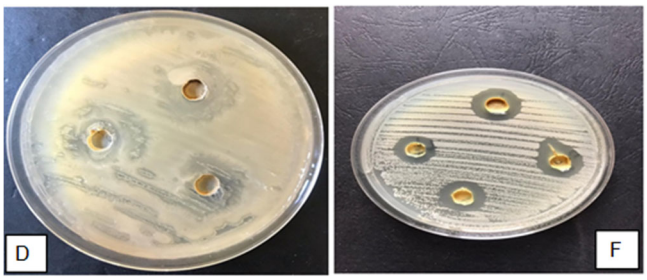

Fig 10. Effect of the prepared compound on growth *S. epidermis*

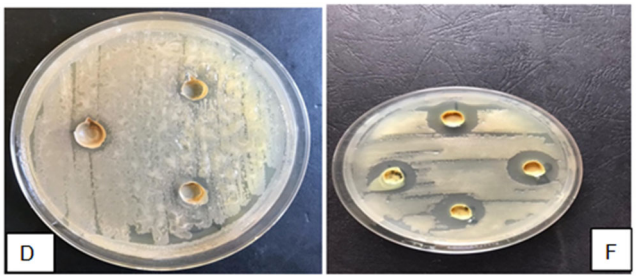

Fig 11. Effect of the prepared compound on growth *S. epidermis*

Table 9. The inhibition zones resulting from the biological activity of compounds D and F

No	Compounds	Concentration (mg mL^{-1})	Inhibition zone (mm)	
			S. epidermis	*E. coli*
1	D	3000	19	20
2	F	3000	0	14

■ CONCLUSION

In summary, the test medium used is a very strong acid of 2 M HCl and thus corrosive to the carbon steel alloy. The heterocyclic and heterocyclic cationic Gemini surfactants inhibitors were found effective by providing a protective film barrier, emanating from the heteroatom's adsorption and the positive quaternary ammonium nitrogen molecules adsorption on the metal surface thus preventing the metal surface test solution interactive corrosion reactions. At all of the concentrations used, the inhibitors D, E, and F gave relatively good and effective protection against corrosion HCl, which was confirmed by electrochemical results. However, the highest concentration of the inhibitor gave the best corrosion inhibition performance at 25 °C. The inhibition efficiency revealed that the decline in %IE occurs in the

following order: F > E > D. The results indicated the biological impact of several chemical solutions made from it with the bacteria under study at 1000 ppm. Compound D was efficient against both types of negative bacteria with a diameter of 20 mm against *E. coli* bacteria and 19 mm *S. epidermis* bacteria at a dosage of 3000 mcg mL^{-1}. With an inhibition diameter of 14 mm, compound F is only effective against *E. coli* at the same dose.

ACKNOWLEDGMENTS

The Laboratory Department in Basra Oil Company (BOC) appreciates the support offered in carrying out this research work.

REFERENCES

[1] Khabibullina, G.R., Fedotova, E.S., Anpilogova, G.R., Akhmetova, V.R., and Ibragimov, A.G., 2016, Multicomponent cyclothiomethylation of phenylenediamines and 4,4'-diaminodiphenyls with formaldehyde and 1,2-ethanedithiol, *Russ. J. Gen. Chem.*, 86, 1608–1612.

[2] Akhmetova, V.R., Khairullina, R.R., Tyumkina, T.V., Nelyubina, Y.V., Smol'yakov, A.F., Bushmarinov, I.S., Starikova, Z.A., Abdullin, M.F., and Kunakova, R.V., 2010, Cyclothiomethylation of carboxylic acid hydrazides with aldehydes and H_2S, *Russ. Chem. Bull.*, 59 (2), 425–433.

[3] Liu, Y., Zhang, H., Liu, Y., Li, J., and Li, W., 2019, Inhibitive effect of quaternary ammonium-type surfactants on the self-corrosion of the anode in alkaline aluminium-air battery, *J. Power Sources*, 434, 226723.

[4] Pakiet, M., Kowalczyk, I., Leiva Garcia, R., Akid, R., and Brycki, B., 2020, Cationic clevelable surfactants as highly efficient corrosion inhibitors of stainless steel AISI 304: Electrochemical study, *J. Mol. Liq.*, 315, 113675.

[5] Kamal, M.S., Hussein, I., Mahmoud, M., Sultan, A.S., and Saad, M.A.S., 2018, Oilfield scale formation and chemical removal: A review, *J. Pet. Sci. Eng.*, 171, 127–139.

[6] Liu, D., Quan, X., Zhu, H., Huang, Q., and Zhou, L., 2020, Evaluation of modified waste concrete powder used as a novel phosphorus remover, *J. Cleaner Prod.*, 257, 120646.

[7] Tung, N.T., Tran, C.S., Nguyen, T.L., Pham, T.M.H., Chi, S.C., Nguyen, H.A., Bui, Q.D., Bui, D.N., and Tran, T.Q., 2021, Effect of surfactant on the *in vitro* dissolution and the oral bioavailability of a weakly basic drug from an amorphous solid dispersion, *Eur. J. Pharm. Sci.*, 162, 105836.

[8] Dandigunta, B., Karthick, A., Chattopadhyay, P., and Dhoble, A.S., 2019, Impact of temperature and surfactant addition on milk foams, *J. Food Eng.*, 299, 110509.

[9] Saad, M.A., Abdurahman, N.H., and Mohd Yunus, R., 2021, Synthesis, characterization, and demulsification of water in crude oil emulsion via a corn oil-based demulsifier, *Mater. Today: Proc.*, 42, 251–258.

[10] Lei, Z., Gao H., Chang, X., Zhang, L., Wen, X., and Wang, Y., 2020, An application of green surfactant synergistically metal supported cordierite catalyst in denitration of selective catalytic oxidation, *J. Cleaner Prod.*, 249, 119307.

[11] Vimal Kumar, K., and Appa Rao, B.V., 2019, Phosphorylated xanthan gum, an environment-friendly, efficient inhibitor for mild steel corrosion in aqueous 200 ppm NaCl, *Mater. Today: Proc.*, 15, 155–165.

[12] Azzam, E.M., Abd El-Salam, H.M., Mohamed, R.A., Shaban, S.M., and Shokry, A., 2018, Control the corrosion of mild steel using synthesized polymers based on polyacrylamide, *Egypt. J. Pet.*, 27 (4), 897–910.

[13] Fouda, A.E.A.S., Abd el-Maksoud, S.A., El-Sayed, E.H., Elbaz, H.A., and Abousalem, A.S., 2021, Effectiveness of some novel heterocyclic compounds as corrosion inhibitors for carbon steel in 1 M HCl using practical and theoretical methods, *RSC Adv.*, 11 (31), 19294–19309.

[14] Akhmetova, V.R., Niatshina, Z.T., Starikova, Z.A., Korzhova, L.F., and Ibragimov, A.G., 2011, Thiomethylation of heteroaromatic amines, *Russ. J. Org. Chem.*, 47 (6), 920–927.

[15] Akhmetova, V.R., and Rakhimova, E.B., 2014, One-pot cyclothiomethylation of amines as efficient method for the synthesis of saturated five-, six-, seven-, and eight-membered *S*,*N*-heterocycles, *Russ. J. Org. Chem.*, 50, 1711–1731.

[16] Akhmetova, V.R., Nadyrgulova, G.R., Niatshina, Z.T., and Dzhemilev, U.M., 2009, Cyclothiomethylation of primary amines with formaldehyde and hydrogen sulfide to nitrogen- and sulfur-containing heterocycles (Review), *Chem. Heterocycl. Compd.*, 45, 1155–1176.

[17] Shaban, S.M., and Elsharif, A.M., Elged, A.H., Eluskkary, M.M., Aiad, I., and Soliman, E.A., 2021, Some new phospho-zwitterionic Gemini surfactants as corrosion inhibitors for carbon steel in 1.0 M HCl solution, *Environ. Technol. Innovation*, 24, 102051.

[18] Khafizova, S.R., Akhmetova, V.R., Kunakova, R.V., and Dzhemilev, U.M., 2003, Thiomethylation of aromatic amines: Efficient method for the synthesis of heterocyclic compounds, *Russ. Chem. Bull.*, 52 (8), 817–1821.

[19] Akhmetova, V.R., Akhmadiev, N.S., and Ibragimov, A.G., 2016, Catalytic multimolecular reactions of 1,3-dicarbonyl CH acids with CH_2O and *S*- and *N*-nucleophiles, *Russ. Chem. Bull.*, 65 (7), 1653–1666.

[20] Akhmetova, V.R., Khabibullina, G.R., Galimzyanova, N.F., and Ibragimov, A.G., 2014, One-pot synthesis and fungicidal activity of 2-(1,5,3-dithiazepan-3-yl)ethanol and *N*,*N*′-bis(2-hydroxyethyl)tetrathiadiazacycloalkanes, *Russ. J. Appl. Chem.*, 87 (3) 294–298.

[21] Akhmetova, V.R., Khairullina, R.R., Nadyrgulova, G.R., Kunakova, R.V., and Dzhemilev, U.M., 2008, Multicomponent heterocyclization of carboxamides with H_2S and CH_2O, *Russ. J. Org. Chem.*, 44 (2), 190–196.

[22] Wang, D., Li, Y., Chen, B., and Zhang, L., 2020, Novel surfactants as green corrosion inhibitors for mild steel in 15% HCl: Experimental and theoretical studies, *Chem. Eng. J.*, 402, 126219.

[23] Loto, C.A., Fayomi, O.S.I., Loto, R.T., and Popoola, A.P.I., 2019, Potentiodynamic polarization and gravimetric evaluation of corrosion of copper in 2 M H_2SO_4 and its inhibition with ammonium dichromate, *Procedia Manuf.*, 35, 413–418.

[24] Akhmetova, V.R., Akhmadiev, N.S., Zainullin, R.A., Khayrullina, V.R., Mescheryakova, E.S., and Glushkova, N.A., 2020, Synthesis, *in vitro* and *in silico* studies of inhibitory activity towards α-amylase of *bis*-azole scaffolds linked by an alkylsulfanyl chain, *Can. J. Chem.*, 98 (11), 725–735.

[25] Flitt, H.J., and Schweinsberg, D.P., 2005, Evaluation of corrosion rate from polarisation curves not exhibiting a Tafel region, *Corros. Sci.*, 47 (12), 3034–3052.

[26] Markhali, B.P., Naderi, R., Mahdavian, M., Sayebani, M., and Arman, S.Y., 2013, Electrochemical impedance spectroscopy and electrochemical noise measurements as tools to evaluate corrosion inhibition of azole compounds on stainless steel in acidic media, *Corros. Sci.,* 75, 269–279.

[27] Solomon, M.M., and Umoren, S.A., 2015, Electrochemical and gravimetric measurements of inhibition of aluminum corrosion by poly (methacrylic acid) in H_2SO_4 solution and synergistic effect of iodide ions, *Measurement*, 76, 104–116.

[28] Liu, Y., Liu, Z., Xu, A., and Liu, X., 2022, Understanding pitting corrosion behavior of AZ91 alloy and its MAO coating in 3.5% NaCl solution by cyclic potentiodynamic polarization, *J. Magnesium Alloys*, 10 (5), 1368–1380.

[29] El Hajjaji, F., Belghiti, M.E., Drissi, M., Fahim, M., Salim, R., Hammouti, B., Taleb, M., and Nahlé, A., 2019, Electrochemical, quantum calculations and Monte Carlo simulation studies of *N1*,*N2*-bis(1-phenylethylidene)ethane-1,2-diamine as a corrosion inhibitor for carbon steel in a 1.0 M hydrochloric acid solution, *Port. Electrochim. Acta*, 37 (1), 23–42.

[30] El Basiony, N.M., Badr, E.E., Baker, S.A., and El-Tabei, A.S., 2021, Experimental and theoretical (DFT & MC) studies for the adsorption of the synthesized Gemini cationic surfactant based on hydrazide moiety as X-65 steel acid corrosion inhibitor, *Appl. Surf. Sci.*, 539, 148246.

[31] Elged, A.H., Shabana, S.M., Eluskkary, M.M., Aiad, I., Soliman, E.A., Elsharif, A.M., and Kim, D.H.,

2021, Impact of hydrophobic tails of new phospho-zwitterionic surfactants on the structure, catalytic, and biological activities of AgNPs, *J. Ind. Eng. Chem.*, 94, 435–447.

[32] Fouda, A.S., Elmorsi, M.A., Shaban, S.M., Fayed, T., and Azazy, O., 2018, Evaluation of *N*-(3-(dimethyl hexadecyl ammonio)propyl) palmitamide bromide as cationic surfactant corrosion inhibitor for API N80 steel in acidic environment, *Egypt. J. Pet.*, 27 (4), 683–694.

[33] Abd-Elaal, A.A., Elbasiony, N.M., Shaban, S.M., and Zaki, E.G., 2018, Studying the corrosion inhibition of some prepared nonionic surfactants based on 3-(4-hydroxyphenyl) propanoic acid and estimating the influence of silver nanoparticles on the surface parameters, *J. Mol. Liq.*, 249, 304–317.

[34] Mobin, M., and Aslam, R., 2018, Experimental and theoretical study on corrosion inhibition performance of environmentally benign non-ionic surfactants for mild steel in 3.5% NaCl solution, *Process Saf. Environ. Prot.*, 114, 279–295.

[35] Aiad, I., Shaban, S.M., Elged, A.H., and Aljoboury, O.H., 2018, Cationic surfactant based on alignate as green corrosion inhibitors for the mild steel in 1.0 M HCl, *Egypt. J. Pet.*, 27, 877–885.

[36] Deyab, M.A., 2019, Enhancement of corrosion resistance in MSF desalination plants during acid cleaning operation by cationic surfactant, *Desalination*, 456, 32–37.

[37] Zhou, T., Yuan, J., Zhang, Z., Xin, X., and Xu, G., 2019, The comparison of imidazolium Gemini surfactant [C_{14}-4-C_{14}im]Br_2 and its corresponding monomer as corrosion inhibitors for A3 carbon steel in hydrochloric acid solutions: Experimental and quantum chemical studies, *Colloids Surf., A*, 575, 57–65.

[38] Shaban, S.M., Abd Elsamad, S., Tawfik, S.M., Abdel-Rahman, A.A.H., and Aiad, I., 2020, Studying surface and thermodynamic behavior of a new multi-hydroxyl Gemini cationic surfactant and investigating their performance as corrosion inhibitor and biocide, *J. Mol. Liq.*, 316, 113881.

[39] Chafiq, M., Chaouiki, A., Damej, M., Lgaz, H., Salghi, R., Ali, I.H., Benmessaoud, M., Masroor, S., and Chung, I.M., 2020, Bolaamphiphile-class surfactants as corrosion inhibitor model compounds against acid corrosion of mild steel, *J. Mol. Liq.*, 309, 113070.

[40] Wang, J., Liu, D., Cao, S., Pan, S., Luo, H., Wang, T., Ding, H., Mamba, B.B., and Gui, J., 2020, Inhibition effect of monomeric/polymerized imidazole zwitterions as corrosion inhibitors for carbon steel in acid medium, *J. Mol. Liq.*, 312, 113436.

[41] Srivastava, V., Haque, J., Verma, C., Singh, P., Lgaz, H., Salghi, R., and Quraishi, M.A., 2017, Amino acid-based imidazolium zwitterions as novel and green corrosion inhibitors for mild steel: Experimental, DFT and MD studies, *J. Mol. Liq.*, 244, 340–352.

[42] Arabahmadi, R., 2019, Cobalt(II) complexes derived from azo-azomethine ligands: Synthesis, characterization, solvatochromic, fluorescence, thermal, electrochemical and antimicrobial properties, *ChemistrySelect*, 4 (17), 4883–4891.

[43] Azam, M., Al-Resayes, S.I., Wabaidur, S.M., Altaf, M., Chaurasia, B., Alam, M., Shukla, S.N., Gaur, P., Albaqami, N.T.M., Islam, M.S., and Park, S., 2018, Synthesis, structural characterization and antimicrobial activity of Cu(II) and Fe(III) complexes incorporating azo-azomethine ligand, *Molecules*, 23 (4), 813.

[44] Fontana, M.G., and Staehle, R.W., 1980, "Biological Corrosion" in *Advances in Corrosion Science and Technology*, 1st Ed., Springer, New York, 1–42.

[45] Jone Kirubavathy, S., and Chitra, S., 2017, Structural, theoretical investigations and biological evaluation of Cu(II), Ni(II) and Co(II) complexes of mercapto-pyrimidine Schiff bases, *J. Mol. Struct.*, 1147, 797–809.

[46] Zorofchian Moghadamtousi, S., Abdul Kadir, H., Hassandarvish, P., Tajik, H., Abubakar, S., and Zandi, K., 2014, A review on antibacterial, antiviral, and antifungal activity of curcumin, *BioMed Res. Int.*, 2014, 186864.